Research Article

Bio-sourced Black Soldier Fly (*Hermetia illucens*) Maggot Chitosan/PVA/PAN-based Polymer Electrolyte Membrane for Sustainable Energy Storage Applications

Muhammad Thoriq Al Fath*, Nisaul Fadilah Dalimunthe, Rivaldi Sidabutar, Michael, Rosma Natalia Samosir and Thiodorus Marvin Tjandra
Department of Chemical Engineering, Faculty of Engineering, Universitas Sumatera Utara, Padang Bulan, Medan, Indonesia

Gina Cynthia Raphita Hasibuan
Department of Civil Engineering, Faculty of Engineering, Universitas Sumatera Utara, Padang Bulan, Medan, Indonesia

* Corresponding author. E-mail: thoriq@usu.ac.id DOI: 10.14416/j.asep.2024.07.002
Received: 7 March 2024; Revised: 19 April 2024; Accepted: 8 May 2024; Published online: 4 July 2024

Abstract
The global energy crisis sparked by dwindling fossil fuel reserves has precipitated efforts to develop sustainable battery technologies, as conventional dry cell batteries utilize toxic lead, graphite, and manganese oxide components that pollute the environment. Chitosan derived from black soldier fly (*Hermetia illucens*) maggot presents a biodegradable substitute. This study fabricated chitosan-based polymer electrolyte membranes by blending chitosan with polyvinyl alcohol (PVA) and polyacrylonitrile (PAN), then doping with ammonium chloride (NH_4Cl) using the solvent-casting method. Varying NH_4Cl compositions aimed to maximize ionic conductivity. Chitosan (13.455% water, 27.810% ash) was subsequently combined with PVA/PAN (20:80 w/w), NH_4Cl, and casted onto petri dishes. Electrolyte membranes exhibited a maximum conductivity of 0.19612 ± 0.01572 S/cm with 0.9 g NH_4Cl. FTIR spectroscopy verified the incorporation of chitosan (peaks at 3446.79 cm^{-1}, 1643.35 cm^{-1}, and 1151.50 cm^{-1}), PVA (3446.79 cm^{-1} and 1136.07 cm^{-1}), and NH_4Cl (3371.57 cm^{-1} and 721.38 cm^{-1}). SEM imaging visualized the incorporation of NH_4Cl within the membrane. The chitosan-based biodegradable approach is compelling but limited by 0.19612 S/cm ionic conductivity, necessitating further compositional and processing optimizations for viable applications. Though it is promising for sustainable bio-sourced energy storage, challenges remain in enhancing conductivity through advanced polymer blends/dopants and scaling up for commercial biobattery manufacturing.

Keywords: Black soldier fly, Chitosan-based biobattery, Dopant, Ionic conductivity, Polymer electrolyte membrane

1 Introduction

Indonesia, as well as the global community, heavily relies on electrical energy for day-to-day activities. Throughout the years, the use of electrical power has significantly increased making it a necessity for human existence. However, conventional electricity derived from non-renewable fossil fuels lacks novelty and sustainability, therefore numerous alternative solutions have been created and developed to address the issue, such as the use of alternative energy sources that are renewable [1]. A battery is an electronic device that produces electricity through conversion of chemical energy from electrochemical reduction and oxidation reactions, also called redox reactions. Electrochemical charge transfer reactions take place at the boundary between electrodes and the electrolyte. These reactions transform chemical energy into electrical energy, serving as a power source for diverse electronic devices. The chemical energy sources mainly originated from heavy metals such as mercury, nickel, etc. Extensive utilization can result in a rise in

heavy metal waste, posing significant environmental hazards [2]. Conventional batteries rely heavily on non-renewable fossil fuels and toxic heavy metals, which lack sustainability and pose significant environmental hazards through greenhouse gas emissions and hazardous waste. Therefore, there is an urgent need to develop environmentally friendly, sustainable alternatives like biobatteries derived from organic materials. Lately, there has been extensive research on natural polymer materials as potential polymer electrolytes due to their environmentally friendly characteristics. Among these, chitosan stands out as one of the most extensively studied natural polymers [3].

Chitosan is a natural polymer chitin derivative that can be used as a proton conducting membrane [4]. Chitosan exhibits good electrical conductivity and can be combined with other polymer materials to further enhance its mechanical properties. Polyvinyl Alcohol (PVA) is widely used as a combination alongside chitosan due to its mechanical properties. Nevertheless, there is poor miscibility between chitosan and PVA, therefore a cross linker agent, such as glutaraldehyde is added to enhance the polymer's properties [5]. Another polymer that has been receiving attention is polyacrylonitrile (PAN) due to its high thermal stability, which is an essential aspect of a battery [6]. In a study by Nofal *et al*., polymer electrolytes have negatively charged groups and the charge carriers of these systems are H^+ ions, which could be obtained from the dissociation of various ammonium salts, including ammonium bromide (NH_4Br), ammonium iodide (NH_4I), and ammonium chloride (NH_4Cl). Research conducted by Yusof *et al*., indicates that an addition of ammonium salt dopant such as NH_4Br could increase the conductivity of chitosan-based polymer electrolyte.

Based on the research studies that have been examined, it is possible to enhance the conductivity of chitosan-based electrolytes through modifications. In this research, the mixture of chitosan-PVA-PAN-Glutaraldehyde will be mixed with ammonium chloride and cast onto a petri dish to produce a solid electrolyte. Additionally, Scanning Electron Microscope (SEM) and the chemical structures of the produced polymer electrolyte will be analyzed using Fourier Transform Infrared Spectrophotometry (FTIR). This research aims to determine the conductivity value of polymer electrolytes derived from the variation of chitosan added with PVA-PAN-Glutaraldehyde and the addition of ammonium chloride salt (NH_4Cl). Furthermore, this research will utilize chitosan as a natural polymer to reduce chemical energy waste in battery production.

2 Materials and Methods

2.1 *Preparation of BSF Chitosan*

The chitosan polymer used in this research was extracted from black soldier fly's (BSF) maggots. As a maggot grows, it has to shed its outer skin called exuviae, which is abundantly available as chitosan-rich waste feedstock. BSF exuviae were first collected from a local maggot cultivator in Medan, Indonesia. The exuviae were subjected to a cleansing procedure comprising three repetitive wash cycles with filtered tap water. The procedure was conducted to eliminate particulate impurities from the exuviae material. Following the aqueous cleansing procedure, the resultant washed exuviae were dried under sunlight exposure. The chitosan was obtained via three stages of extraction and purification procedure: deproteination (to break down and remove protein contents from BSF), demineralization (to dissolve and remove mineral contents from BSF), and deacetylation (treating chitin using a strong base at high temperatures to remove the acetyl groups from the chitin molecules, resulting in the formation of chitosan). Subsequent assaying to quantify water and ash content was conducted on the extracted chitosan product. Additionally, the functional groups of the obtained chitin and chitosan were analyzed using a Fourier Transform Infrared (FTIR) spectrometer.

2.2 *Determination of ash and water content*

The ash and water content of the produced chitosan were tested in the Integrated Laboratory, Universitas Sumatera Utara. Ash content serves as a critical analytical aspect to determine the purity and quality attributes of the derived chitosan product. Lower measurable ash content corresponds to higher quality chitosan [7]. The ash content was calculated as a function of the residual to initial mass via the mathematical expression in the Equation (1).

$$\% \text{ Ash content} = \frac{w_3 - w_1}{w_2 - w_1} \times 100\% \quad (1)$$

where, w_3 is the weight of chitosan ash and petri dish, w_2 is the weight of chitosan and petri dish, and w_1 is the weight of only the petri dish.

Water content was also evaluated using the following mathematical formula in the Equation (2).

$$\% \text{ Water content} = \frac{w_1 - w_2}{w_1} \times 100\% \quad (2)$$

where, w_1 is the weight of the sample before drying and w_2 is the constant weight obtained after drying [8].

2.3 *Fabrication of Chitosan/PVA/PAN/NH_4Cl polymer electrolyte membrane*

The fabrication of the membranes commenced by mixing 1.2 g of PVA/PAN composites prepared in two distinct ratios, 10:90 and 20:80, respectively. Chitosan was added into the PVA/PAN mixtures at varying quantities of 2.4; 2.8; and 3.2 g. The mixtures were heated at 80 ºC for 5 min under constant agitation at 500 rpm using a magnetic stirrer apparatus. The solutions were then rapidly cooled to 25 ºC. Next, 1 mL of 6% (v/v) glutaraldehyde was added and extensively mixed for 15 min. The procedure was followed by the incorporation of 0.4 g of ammonium chloride salt (NH_4Cl) into the mixture. After attaining homogenized solution, the final solutions were casted onto a petri dish and dried using a Memmert, E1515E laboratory drying oven at 60 ºC for 15 h.

Fabrication of bio-battery assemblies was carried out in the Organic Chemistry Laboratory, Chemical Engineering, Faculty of Engineering, Universitas Sumatera Utara, using the developed polymer electrolyte membranes comprising of chitosan/PVA/PAN/NH_4Cl to ascertain the obtained voltage outputs as a function of composition. Residual graphite material from spent zinc-carbon AA dry cell was extracted and cleaned. Subsequently, the purified graphite was then enveloped in the rolled membrane structures to achieve complete encapsulation. Then, a quantitative assay of the bio-battery electrical performance parameters was measured using a multimeter.

2.4 *Measurement of Membrane Conductivity*

Based on the electrical conductivity performance, the chitosan/PVA/PAN membrane exhibiting the maximum variation was selected as the optimum composition for subsequent testing with incrementally amended NH_4Cl content (0; 0.3; 0.6; 0.9; and 1.2 g). The produced polymer membranes were then quantitatively assayed for electrical conductivity using a multimeter (Junejour Digital, XL830L). Scanning Electron Microscopy (SEM) analysis was carried out, using a machine model (HITACHI TM 300) to provide cross-sectional morphological visualization of the produced membrane.

Measurements were carried out using DC current and after obtaining the value conductivity can be calculated using Equation (3).

$$\sigma = \frac{IL}{V\pi r^2} \quad (3)$$

where σ is the electrical conductivity ($S.cm^{-1}$), I is the value of the current measured (A), V is the voltage (V), L is the thickness of the membrane (cm), and r is the radius of the membrane (cm) [9].

3 Results and Discussions

3.1 *Characterization of BSF-based Chitosan*

Chitosan was derived from BSF biomass and characterized to quantify water and ash content. Throughout the bioconversion process to transform BSF into chitosan, the percentage yield at each stage was reported. The graphical representation in Figure 1 visualizes the stepwise yield obtained during the chitin-to-chitosan conversion procedure.

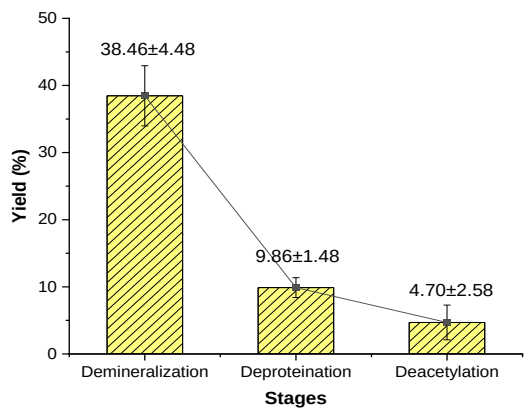

Figure 1: Yield of chitosan in each stage.

The conversion yield indicates a stepwise decrease in product recovery at each sequential stage of processing BSF biomass to chitosan. The percentage yield obtained post-demineralization was quantified as 38.46 ± 4.48% relative to the initial BSF feedstock. Following deproteination, an additional decrease in process yield to 9.86 ± 1.48%. The final

yield after the deacetylation process measured 4.70 ± 2.58% in reference to the initial BSF feedstock input.

The quantitatively determined percentages for water and ash contents in the synthesized chitosan are 13.455% and 27.810%. A high ash content negatively can impact properties such as solubility and viscosity. Ash content serves as an indicator of the effectiveness of the demineralization process used to purify chitosan. The lower ash content refers to a purer form of chitosan that has a greater proportion of minerals removed. Ash content analysis qualifies the level of residual inorganic material that remains within chitosan. The amount of ash in a substance could be used to measure how soluble chitosan was in certain solvents. When the ash content is high, it signals high residual mineral levels and therefore poorer solubility and solution viscosity [10].

Water content serves as a quality metric for chitosan, as it impacts the material's susceptibility to microbial growth. Several factors influence the water content, including drying methods, duration of drying, batch size, and contact surface area. The high level of water content observed in this study is believed to stem from atmospheric water absorption. This is because chitosan contains amino groups that have the ability to bind water molecules from their surroundings. Additionally, the ash content of the chitosan reached just 27.81%. Ash content level holds importance as a key to chitosan parameter. The low ash residue signifies an effective demineralization process during production, leaving behind a small amount of inorganic mineral components. In summary, while moisture content was elevated due to atmospheric water uptake, ash content analysis confirms the high purity of the chitosan sample based on depleted mineral levels in the chitosan itself [10], [11].

3.2 *FTIR Analysis on Extracted Chitin and Chitosan*

FTIR spectroscopic characterization was performed on both chitin and chitosan obtained post-extraction to identify predominant functional group present. The spectral acquisitions were recorded over an extended wavelength from 4000 cm^{-1} to 400 cm^{-1} as shown in Figure 2.

Table 1 shows functional group for both chitosan and chitin. The carbon bond on chitin has a large range of wave absorbance on the fingerprint zone, making it difficult to interpret. Chitin's infrared spectrum shows nine main peaks at 445.56; 1031.92; 1161.15; 1234.44; 1529.55; 1645.28; 2376.3; 2924.09; and 3414 cm^{-1}. The characteristic marker of the produced chitin was found on the peak of 2924.09 cm^{-1}, and the presence of a standard chitin spectrum indicates the vibration of N-H bonds that is the part of amine groups.

The FTIR spectrum of the chitosan product exhibited six absorption peaks at wavenumbers (cm^{-1}) at 1028.06; 1558.48; 1653.00; 2414.88; 2920.23; and 3471.87. The reaction of forming chitosan from chitin is a hydrolysis reaction of an amide by a base. Chitin acts as the amide and NaOH as the base. Based on the result of the analysis, the peak at 1653.00 cm^{-1} indicates the presence of the amide group which is the absorption band of C=O bond group. Then, at the peak of 3471.87 cm^{-1}, indicates the vibration of O-H and N-H bond group. According to Rachmawaty *et al.*, the result of FTIR spectrum of chitosan material consists of several functional groups such as OH, NH, CH, C=O, CO, CN, COC, and β-1,4-glycosidic [12].

The spectrum analysis indicates characteristic structural transitions from chitin to chitosan, indicated by the presence of the amide and hydroxyl functional groups. The peak at 2920.23 cm^{-1} corresponds to alkane (C-H) stretching vibrations. Additionally, the peak at 3471.87 cm^{-1} represents overlapping absorptions of hydroxyl (O-H) and amine (N-H) moieties. Supplementary to the observed spectral features, the formation of chitosan can be verified by a decreased absorption intensity around 1600 cm^{-1} region compared to the FTIR spectrum result of the chitin precursor. This reduction in amide carbonyl intensity signifies the hydrolysis of amide groups during the conversion of chitin to chitosan [13].

3.3 *Electrical conductivity*

Determination of the electrical conductivity was done using a multimeter. The polymer electrolyte was used to coat the graphite rod from the AA zinc-carbon battery. The thickness of the polymer used to coat the rod fully is 0.45 cm. The polymer thickness used was measured using an anvil-sized membrane.

Conductivity value is first conducted to determine the optimum membrane conductivity with chitosan variations (2.4; 2.8; and 3.2 g) and PVA/PAN compositions (10:90 and 20:80). The result is presented in Table 2.

The maximum conductivity value was attained in the PVA/PAN blend composition of 20:80, with the addition of 2.4 g chitosan. The incorporation of PVA/PAN mixture improved the ionic conductivity

and mechanical properties of the chitosan-based polymer electrolyte. A maximum conductivity of 0.16740 $S.cm^{-1}$ was achieved using the 20:80 PVA/PAN ratio with 2.4 g chitosan. This indicates that increasing the PVA composition results in higher conductivity. This can be attributed to the highly hydrophilic characteristics of PVA with a large presence of hydroxyl group along its backbone. Its feature promotes great affinity to water which could make a desirable contribution to promoting ion conduction in aqueous-based solid polymer electrolytes [14]. Conversely, PAN with its hydrophobic nature of a long alkyl chain will reduce the hydrophilicity of the polymer blend [15]. The integration of PAN segments into PVA helps prevent excessive water absorption. Excessive hydration can deteriorate the interactions between polymer chains due to the high volume of water molecules occupying free space between chains causing swelling, loss of mechanical strength, decreased oxidative stability, and increased permeabilities [16].

The electrical conductivity of prepared polymer electrolyte membranes also revealed there was a decrease in conductivity with increasing chitosan content for all PVA/PAN ratios. This observation can be attributed to the poor chitosan's electrical properties due to its polysaccharide structure lacking free electrons. The polysaccharide structure of chitosan held together by covalent bonds which makes the electrons are locked in these bonds and inhibits the flow of electric current [17]. In the 10:90 PVA/PAN blend, the conductivity showed a consistent declining trend as the composition of electrically non-conductive chitosan composition was increased.

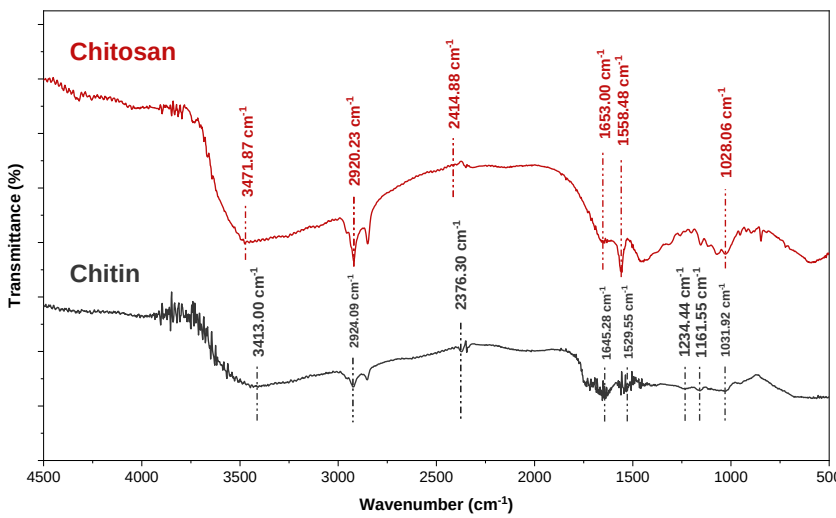

Figure 2: Chitin and chitosan FTIR result.

Table 1: Functional groups of chitin and chitosan from FTIR analysis.

No	Sample	Wavenumber (cm^{-1})	Functional Groups	Wavenumber Range (cm^{-1})
1	Chitin	1031.92	C-C stretch	1300–700
		1161.15	C-C stretch	1300–700
		1234.44	C-C stretch	1300–700
		1529.55	C=C-C stretch	1510–1450
		1645.28	N-H bend	1650–1550
		2376.30	O=C=O stretch	2400–2000
		2924.09	C-H	2935–2915
		3414.00	O-H	3400–3200
2	Chitosan	1028.06	C-O-C stretch	1000–1350
		1558.48	C-H stretch	1300–1567
		1653.00	C=O	1630–1690
		2414.88	C-H aromatic	2100–2550
		2920.23	C-H aliphatic	2850–2970
		3471.87	O-H bend; N-H stretch	3000–3500

The stepwise addition of chitosan is expected to hinder the mobility of ionic charge. Moreover, for a higher PVA/PAN ratio (20:80), the reduction in conductivity was found subtler (0.16740 $S.cm^{-1}$ to 0.14147 $S.cm^{-1}$) despite the same rise in chitosan addition. This finding implies that higher PVA content helps mitigate the loss of conductivity associated with chitosan inclusion. The hydroxyl groups of PVA can promote ion dissociation, partially compensating for the diminished ion mobility imposed by the non-conductive chitosan [14].

The polymer membrane with the maximum conductivity from prior tests (PVA/PAN ratio of 20:80 and 2.4 g chitosan) was selected for additional modification with varying NH_4Cl compositions of 0, 0.3, 0.6, 0.9, and 1.2 g to determine the optimal NH_4Cl loading.

Table 2: Conductivity of polymer electrolyte membrane with varying PVA/PAN ration and chitosan content.

PVA/PAN (1.2 g)	Chitosan (g)	NH_4Cl (g)	Conductivity ($S.cm^{-1}$)
10:90	2.4	0.4	0.12837
	2.8		0.05836
	3.2		0.05153
20:80	2.4		**0.16740**
	2.8		0.05043
	3.2		0.14147

Table 3: Conductivity of selected polymer electrolyte membrane with NH_4Cl variation.

PVA/PAN (1.2 g)	Chitosan (g)	NH_4Cl (g)	Conductivity ($S.cm^{-1}$)
20:80	2.4	0	0.11664 ± 0.04640
		0.3	0.16370 ± 0.02285
		0.6	0.17018 ± 0.02460
		0.9	**0.19612 ± 0.01572**
		1.2	0.15893 ± 0.03044

The conductivity for each doping composition was summarized in Table 3. Table 3 shows the effect of various NH_4Cl additions to the chitosan/PVA/PAN polymer membrane. Initially, the electrical conductivity exhibited an increase with incremental addition of the NH_4Cl salt up to 0.9 g. The incorporation of the NH_4Cl salt provides additional ionic charge which can improve the ionic conductivity of the polymer segment [3]. However, further increasing the NH_4Cl loading by 0.9 g resulted in a decline in conductivity. The initial rise in conductivity with low NH_4Cl can be attributed to the availability of abundant free ions that contribute to charge transport. Higher salt addition leads to oversaturation and precipitation of salt within the polymer chains. This obstructs ion mobility by impeding chain flexibility and high density solid salt precipitation is expected to hinder ion transport at high NH_4Cl loadings [18]. Thus, the addition of NH_4Cl beyond the optimal composition impaires ion mobility and decreases the overall ionic conductivity of the polymer electrolyte membranes.

3.4 *FTIR analysis on fabricated polymer membrane*

The chemical structure and interaction of membrane composition were characterized using FTIR spectroscopy. Spectroscopic analysis was conducted on both pristine chitosan/PVA/PAN membrane, as well as on membrane with the highest obtained conductivity (0.9 g NH_4Cl dopant addition), denoted as chitosan/PVA/PAN/NH_4Cl membrane. The obtained FTIR spectra of Chitosan/PVA/PAN with and without NH_4Cl is shown in Figure 3.

FTIR analysis of the chitosan/PVA/PAN/NH_4Cl membrane revealed numerous signature vibrational modes attributable to constituent chemical moieties. As depicted in Figure 3, selected absorption peaks or wavenumbers visualized the identified functional groups within the membrane structure. A broad absorption band between 3650 and 3250 cm^{-1} indicates a hydrogen bond, with the intense band at 3446.79 cm^{-1} confirming the existence of a hydroxyl (-OH) group. This result alligns with molecular structure of chitosan, since chitosan consists of three types of functional groups: amino/acetamide, primary, and secondary hydroxyl groups [19]. The absorption wavelengths of other functional groups were also documented in Table 4. The primary and secondary alcohol stretches were subsequently verified at 3645–3630 cm^{-1} and 3635–3620 cm^{-1}, respectively, overlapping the O-H stretch region. Amino was detected at 1680–1630 cm^{-1}, complementing the main structures of chitosan. Additionally, the bending vibrations of primary amine (N-H) at 1643.35 cm^{-1} and C-O stretching vibration at 1151.50 cm^{-1} originate from the chitosan structure [20]. At the same time, signature bands attributable to PVA were evident at 3446.79 cm^{-1} (O-H stretch) and 1136.07 cm^{-1} (C-O stretch) [21]. Collectively, the infrared spectroscopic results confirm the successful integration of chitosan within the membrane structure.

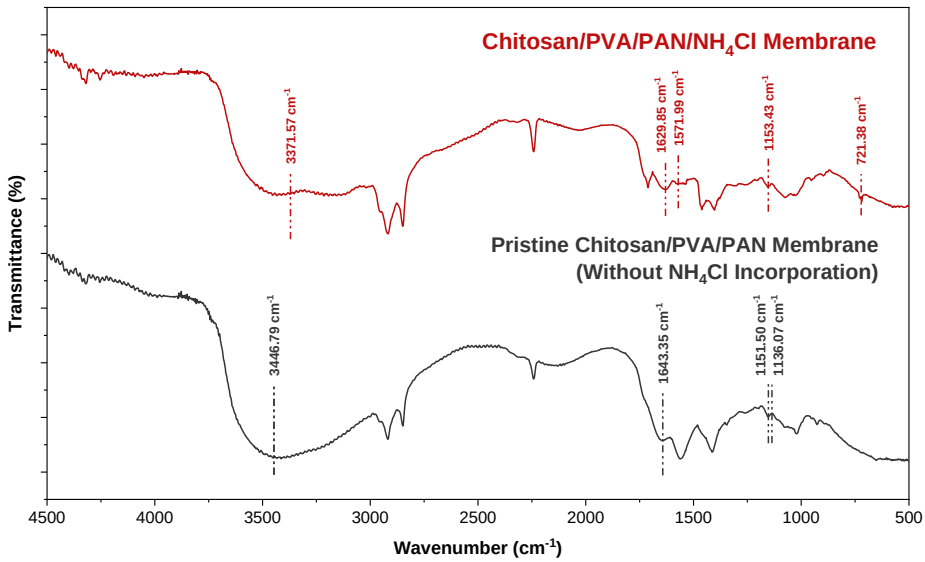

Figure 3: FTIR result of fabricated membrane with and without NH_4Cl.

Table 4: Functional groups of fabricated membranes from FTIR analysis.

No	Membrane	Wavenumber (cm^{-1})	Functional Groups	Wavenumber Range (cm^{-1})
1	Chitosan/ PVA/PAN without NH_4Cl	3446.79	-OH stretch	3600–3000
		3446.79	Aromatic primary amine, N-H stretch	3510–3460
		1643.35	Primary amine, N-H bend	1650–1590
		1151.50	C-O stretch	~1150
		1136.07	Cyclic ethers, C-O stretch	1140–1070
2	Chitosan/ PVA/PAN with NH_4Cl	3371.57	Hydroxy group, H-bonded OH stretch	3570–3200
		1629.85; 1571.99	Secondary amine, >N-H bend	1650–1550
		1153.43	C-O stretch	~1150
		721.38	Aliphatic chloro, C-Cl stretch	800–700

Moreover, the addition of NH_4Cl into the chitosan/PVA/PAN membranes resulted in notable shifts in FTIR spectra. A peak shift was observed at 3371.57 cm^{-1} corresponding to the bonded OH stretch, along with secondary amine bending vibration at around 1629.85 and 1571.99 cm^{-1}. The intensity of these two peaks is associated with N-H bending vibrations in which NH_4Cl incorporation increases its peak intensity compared to pristine chitosan/PVA/PAN membrane. The PVA-signatured C-O stretching vibration was also observed around 1150 cm^{-1}. These results indicate that increasing NH_4Cl incorporation led to a decrease in the PVA peak intensity along with an increase in chitosan absorption intensity in the chitosan/PVA/PAN/NH_4Cl membranes. As described previously [19], chitosan mainly contained amino, primary, and secondary hydroxyl groups, thus NH_4Cl incorporation, which alters the intensity of chitosan functional groups. This is apparent as a decrease in the peak around 1650 cm^{-1} from carbonyl/amide groups in chitosan as NH_4Cl disrupts inter- and intramolecular hydrogen bonds, as well as narrowing -OH stretch in 3600–3000 cm^{-1}, compared to the pristine membrane. Interestingly, the H-bonded OH stretch as detected at wavenumber 3371.57 cm^{-1} indicates complexation between the polymer and ammonium salt. This complexation attributes to H+ ions of ammonium salts acting as the conducting ion and being attracted to the -OH anions of chitosan, forming H-bonded OH group at the region [22]. The previously mentioned N-H bend and additional aliphatic chloro compounds (C-Cl) at 721.38 cm^{-1} prove the presence of NH_4Cl salts in the polymer matrix.

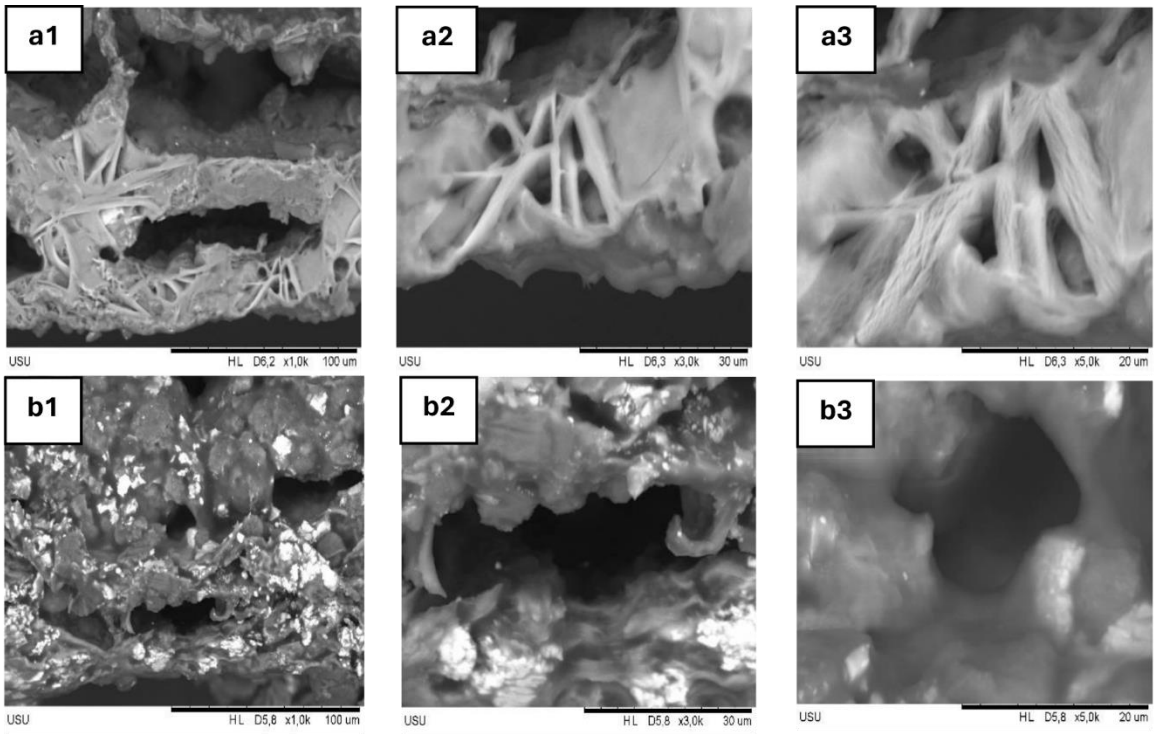

Figure 4: SEM analysis of (a) Membrane without NH_4Cl addition and (b) Membrane with 0.9 g NH_4Cl addition.

3.5 *SEM analysis*

SEM analysis was conducted to determine the morphological structure of the synthesized membrane. SEM imaging was carried out at 1000x, 3000x, and 5000x magnification to evaluate the cross-sectional membrane morphology. Figure 4 illustrates the observed morphological differences in the cross-sectional area of the electrolyte membrane with and without NH_4Cl.

Figure 4(a) exhibits the cross-sectional morphology of the membrane. It can be observed that the membrane structure, which is synthesized without the addition of NH_4Cl consists of uniform pore dimensions and a fibrous structure of a modified polymer electrolyte membrane.

Figure 4(b) displays cross-sectional images of a membrane with 0.9 g of NH_4Cl. The incorporation of this component resulted in a hollow and porous matrix structure. The structure is probably formed due to weak interaction between the filler and the matrix [23]. As described by Ding and Han [24], weakened molecular bonding promotes clump and void space formation, therefore decreasing the density and affecting the porosity properties of the membrane matrix.

Comparative SEM analysis of cross-sectional area distinguishes membranes with and without NH_4Cl incorporation. The chitosan/NH_4Cl coated composite membrane improved its porosity due to the addition of hydrophilic (polar) groups of chitosan and NH_4Cl. Furthermore, the strong hydrogen bonding between chitosan and NH_4Cl significantly stabilizes the composite structure [25].

4 Conclusions

To fabricate a biobattery, chitosan was extracted from BSF (*Hermetia illucens*) and incorporated into a PVA/PAN/NH_4Cl casting solution. The extracted chitosan yielded 4.70 ± 2.58%. FTIR spectroscopy confirmed the successful chitin deacetylation of chitosan. Preliminary testing of the chitosan/PVA/PAN/NH_4Cl polymer electrolyte membranes revealed an optimal PVA/PAN ratio of 20:80. Using this PVA/PAN ratio, NH_4Cl was added as a dopant at various concentrations. The maximum polymer electrolyte membrane conductivity of 0.19612 ± 0.01572 S/cm was achieved with 1.2 g total PVA/PAN (20:80 ratio), 2.4 g chitosan, and 0.9 g NH_4Cl. However, high NH_4Cl concentrations impede ion mobility, which indicates oversaturation. Thus, 0.9 g

NH_4Cl addition was the optimal conductivity. The fabricated membranes were characterized by FTIR and SEM. FTIR verified the successful NH_4Cl integration in the membrane compared to those of the fabricated membrane without NH_4Cl. Additionally, SEM revealed the formation of salt throughout the cross-section of the NH_4Cl-containing membranes. The natural abundance of chitosan enables the fabrication of low-cost and eco-friendly batteries with promising performance. Further optimization of the electrode composition and cell design could enhance the power and energy density. The future research direction is to demonstrate that chitosan-based biobatteries represent a sustainable technology for energy storage.

Acknowledgements

The research was funded by the Institute for Research at Universitas Sumatera Utara (LP-USU) through Applied "Penelitian Terapan" Research scheme, as per research grant number 2837/UN5.1.R/SR/PPM/2023 and decree 13388/UN5.1.R/PPM/2023. The authors sincerely acknowledge and express gratitude for the research sponsorship enabling the presented work.

Author Contributions

M.T.A.F.: funding acquisition, conceptualization, project administration, and reviewing; N.F.D.: funding acquisition and reviewing; R.S.: funding acquisition and reviewing; M.: research design, conceptualization, project administration, and editing; R.N.S.: research idea and data analysis; T.M.T.: research idea, data analysis, and reviewing; G.C.R.H. : Proofreading the article.

Conflict of Interests

The authors declare no conflict of interest.

References

[1] A. S. Ramadana, A. S. Ballqis, Khairunnisa, Lazulva, and Yusbarina, "The potential of bio-battery biomass as an alternative energy source (Review article)," in *International Conference of Humanities and Social Science (ICHSS)*, 2022, pp. 317–327.

[2] G. Rumbino, L. Maniambo, M. Soll, G. Dirgantari, and O. Togibasa, "Performance enhancement of biobattery from tropical almond paste using acetic acid addition," *Indian Journal of Pure & Applied Physics*, vol. 13, no. 1, pp. 99–105, Apr. 2023, doi: 10.13057/ijap.v12i2.61245.

[3] Y. Y. Lim, A. Miskon, and A. M. A. Zaidi, "CuZn complex used in electrical biosensors for drug delivery systems," *Materials*, vol. 15, no. 21, Nov. 2022, doi: 10.3390/ma15217672.

[4] Y. Y. Lim, A. M. A. Zaidi, and A. Miskon, "Composing on-program triggers and on-demand stimuli into biosensor drug carriers in drug delivery systems for programmable arthritis therapy," *Pharmaceuticals*, vol. 15, no. 11, Oct. 2022, doi: 10.3390/ph15111330.

[5] Y. Y. Lim, A. M. A. Zaidi, and A. Miskon, "Combining copper and zinc into a biosensor for anti-chemoresistance and achieving osteosarcoma therapeutic efficacy," *Molecules*, vol. 28, no. 7, Mar. 2023, doi: 10.3390/molecules28072920.

[6] R. Singh, S. Janakiraman, M. Khalifa, S. Anandhan, S. Ghosh, A. Venimadhav, and K. Biswas, "A high thermally stable polyacrylonitrile (PAN)-based gel polymer electrolyte for rechargeable Mg-Ion battery," *Journal of Materials Science: Materials in Electronics*, vol. 31, no. 24, pp. 22912–22925, Nov. 2020, doi: 10.1007/s10854-020-04818-1.

[7] N. D. Takarina, A. B. Indah, A. A. Nasrul, A. Nurmarina, A. Saefumillah, A. Fanani, and K. D. P. Loka, "Optimisation of deacetylation process for chitosan production from red snapper (*Lutjanus* sp.) scale wastes," *International Seminar on Mathematics, Science, and Computer Science Education*, vol. 812, pp. 1–5, 2017, doi: 10.1088/1742-6596/812/1/012110.

[8] A. Fehervari, W. P. Gates, C. Gallage, and F. Collins, "A porous stone technique to measure the initial water uptake by supplementary cementitious materials," *Minerals*, vol. 11, no. 11, Oct. 2021, doi: 10.3390/min11111185.

[9] Y. Gao, J. H. Cho, J. Ryu, and S. Choi, "A scalable yarn-based biobattery for biochemical energy harvesting in smart textiles," *Nano Energy*, vol. 74, no. 1, pp. 1–9, Aug. 2020, doi: 10.1016/j.nanoen.2020.104897.

[10] S. R. Ningrum, S. M. Sinaga, and U. Harahap, "Isolation of chitosan from cuttlefish bones," *International Journal of Science, Technology & Management*, vol. 3, no. 3, pp. 785–788, May 2022, doi: 10.46729/ijstm.v3i3.523.

[11] D. Anggreini, Yuandani, and S. M. Sinaga, "Isolation of chitosan from dogol shrimp skin (*Parapenaeopsis Sculptilis*)," *International Journal of Science, Technology & Management*,

vol. 4, no. 1, pp. 69–72, Jan. 2023, doi: 10.46729/ijstm.v4i1.737.

[12] R. Rachmawaty, S. Sahribulan, S. E. Putri, and W. F. Arisma, "Formation of chitosan from black soldier fly (*hermetia illucens*) pupae using microwaves radiation energy," *Jurnal Aisyah*, vol. 8, no. 2, pp. 1173–1180, Jun. 2023, doi: 10.30604/jika.v8i2.2142.

[13] R. M. Silverstein, X. W. Francis, and J. K. David, *Spectrometric identification of Organic Compound*, 7th ed. Genola, UT: Spring Lake Publishing, 1989.

[14] L. Fan, M. Wang, Z. Zhang, G. Qin, X. Hu, and Q. Chen, "Preparation and characterization of pva alkaline solid polymer electrolyte with addition of bamboo charcoal," *Materials*, vol. 11, no. 5, p. 679, Apr. 2018, doi: 10.3390/ma11050679.

[15] R. Arat, H. Baskan, G. Ozcan, and P. Altay, "Hydrophobic silica-aerogel integrated polyacrylonitrile nanofibers," *Journal of Industrial Textiles*, vol. 51, no. 3, pp. 4740S–4756S, Jun. 2022. doi: 10.1177/1528083720939670.

[16] R. S. Rafidah, W. Rashmi, M. Khalid, W. Y. Wong, and J. Priyanka, "Recent progress in the development of aromatic polymer-based proton exchange membranes for fuel cell applications," *Polymers*, vol. 12, no. 5, May 2020, Art. no. 1061, doi: 10.3390/polym12051061.

[17] S. Dalwadi, A. Goel, C. Kapetanakis, D. S. Cruz, and X. Hu, "The integration of biopolymer-based materials for energy storage applications: A review," *International Journal of Molecular Sciences*, vol. 24, no. 4, Feb. 2023, Art. no. 3975, doi: 10.3390/ijms24043975.

[18] S. S. Azahar, T. S. Hamidon, A. F. A. Latip, and M. H. Hussin, "Physicochemical and conductivity studies of chitosan-tapioca flour-$LiBF_4$ gel polymer electrolytes," *Chemical Physics Impact*, vol. 3, no. 1, Dec. 2021, Art. no. 100055, doi: 10.1016/j.chphi.2021.100055.

[19] M. Yadav, B. Kaushik, G. K. Rao, C. M. Srivastava, and D. Vaya, "Advances and challenges in the use of chitosan and its derivatives in biomedical fields: A review," *Carbohydrate Polymer Technologies and Applications*, vol. 5, Jun. 2023, Art. no. 16150, doi: 10.1016/j.carpta.2023.100323.

[20] F. Khoerunnisa, P. C. Amanda, M. Nurhayati, H. Hendrawan, W. W. Lestari, E. E. Sanjaya, M. Handayani, W-D. Oh, and J. K. Lim, "Promotional effect of ammonium chloride functionalization on the performance of polyethersulfone/chitosan composite-based ultrafiltration membrane," *Chemical Engineering Research and Design*, vol. 190, no. 1, pp. 366–378, Feb. 2023, doi: 10.1016/j.cherd.2022.12.040.

[21] S. Woranuch, A. Pangon, K. Puagsuntia, N. Subjalearndee, and V. Intasanta, "Rice flour-based nanostructures via a water-based system: Transformation from powder to electrospun nanofibers under hydrogen-bonding induced viscosity, crystallinity and improved mechanical property," *RSC Advances*, vol. 2017, no. 7, pp. 19960–19966, Apr. 2017, doi: 10.1039/C7RA01485F.

[22] N. M. Khan, N. S. M. Ali, A. A. A. Fuzlin, and A. S. Salihin, "Ionic conductiviy of alginate-NH_4Cl polymer electrolyte," *Makara Journal of Technology*, vol. 24, no. 3, pp. 125–130, Dec. 2020, doi: 10.7454/mst.v24i3.3841.

[23] M. T. Al Fath, G. E. Ayu, M. Lubis, G. C. R. Hasibuan, and N. F. Dalimunthe, "Mechanical and thermal properties of starch avocado seed bioplastic filled with cellulose nanocrystal (CNC) as filler and potassium chloride (KCl) as dispersion agent," *Rasayan Journal of Chemistry*, vol. 16, no. 3, pp. 1630–1636, Sep. 2023, doi: 10.31788/RJC.2023.1638464.

[24] Z. Li, Q. Ding, and W. Han, "PVA-based high carboxyl group substituted modified cellulose nanofiber composite hydrogel for flexible new air battery PVA-based high carboxyl group substituted modified cellulose nanofiber composite hydrogel for flexible new air battery," in *International Conference on Chemistry and Energy Research*, Jan. 2021, pp. 1–7, doi: 10.1088/1755-1315/639/1/012044.

[25] F. Khoerunnisa, P. C. Amanda, M. Nurhayati, H. Hendrawan, W. W. Lestari, E. H. Sanjaya, M. Handayani, W. D. Oh, and J. K. Lim, "Promotional effect of ammonium chloride functionalization on the performance of polyethersulfone/chitosan composite-based ultrafiltration membrane," *Chemical Engineering Research and Design*, vol. 190, pp. 366–378, Dec. 2022, doi: 10.1016/j.cherd.2022.12.040.